Available online at www.sciencedirect.com
SCIENCE DIRECT®
Bioorganic & Medicinal Chemistry 13 (2005) 1021–1029
Bioorganic & Medicinal Chemistry

Mechanistic study of proton transfer and hysteresis in catalytic antibody 16E7 by site-directed mutagenesis and homology modeling

Lei Zheng,[a] Roman Manetsch,[b,†] Wolf-Dietrich Woggon,[b] Ulrich Baumann[a] and Jean-Louis Reymond[a,*]

[a]*Department of Chemistry and Biochemistry, University of Berne, Freiestrasse 3, CH-3012 Berne, Switzerland*
[b]*Department of Chemistry, University of Basel, St. Johanns-Ring 19, CH-4056 Basel, Switzerland*

Received 11 October 2004; revised 19 November 2004; accepted 22 November 2004
Available online 19 December 2004

Abstract—Antibody 16E7 catalyzes the carbon protonation of enol ether **2** to hemiacetal **3**, and the carbon deprotonation of benzisoxazole **7** to phenol **8**. This antibody shows an extreme case of hysteresis, requiring several hours to reach full activity. Antibody 16E7 was expressed as recombinant chimeric Fab in *Escherichia coli*. A model for the three-dimensional structure was produced by homology modeling and used for a docking procedure to obtain models for antibody–ligand complexes. Site-direct mutagenesis of Glu^{L39}, identified as a possible catalytic residue by the model, to either glutamine or alanine abolished catalysis, showing that both the protonation reaction of enol ether **2** and the deprotonation of benzisoxazole **7** are promoted by the same residue. The model furthermore suggested that substrate access to the catalytic site might be hindered by a flexible HCDR3 loop held in closed position by a hydrogen bond between Ser^{H99} and Glu^{L39}, which could explain the observed hysteresis effect. In agreement with this model, mutagenesis of Ser^{H99} to alanine, or deletion of this residue, was found to reduce hysteresis by approximately 50%.

1. Introduction

Catalytic antibodies can be obtained by immunization against small molecule haptens that are either transition state analogs or reactive probes corresponding to a given reaction.[1] Most catalytic antibodies accelerate base-promoted hydrolytic processes or pericyclic reactions.[2] Catalytic antibodies for carbon protonation and deprotonation reactions are of particular interest due to the fundamental nature of this step, which is the key to catalysis in many natural enzymes.[3] We recently reported the preparation of catalytic antibody 16E7, obtained by immunization against the guanidinium hapten **1**.[4] This antibody catalyzes proton transfer to and from carbon in two separate reactions, which are the acid-promoted protonation of enol ethers **2** to form hemiacetal **3**, and the base-promoted deprotonation of benzisoxazole **7** to form cyanophenol **8** (Fig. 1). Both types of reactions have been previously observed individually in different catalytic antibodies.[5–7] However, no catalytic antibody has been reported previously to catalyze both reaction types within the same binding pocket, which renders the molecular reaction mechanism of antibody 16E7 particularly interesting. In addition, catalytic antibody 16E7 exhibits an unusual case of hysteresis for both its protonation and its deprotonation reactions, whereby catalysis requires several hours to reach full activity in the presence of substrate. This retardation effect is reversible, suggesting an underlying protein dynamics effect.

Herein we report a site-directed mutagenesis study of catalytic antibody 16E7 guided by homology modeling. A three-dimensional model of catalytic antibody 16E7 was produced and used in a docking procedure to generate a model of the antibody complexes with hapten **1** and substrates **2** and **7**. Residue Glu^{L39} was identified as the key catalytic residue responsible for both the protonation and the deprotonation activity of antibody

Keywords: Catalytic antibody; Proton transfer; Homology modeling; Site-directed mutagenesis.
* Corresponding author. Tel.: +41 31 631 4325; fax: +41 31 631 8057; e-mail: jean-louis.reymond@ioc.unibe.ch
† Present address: The Scripps Research Institute, 10550 North Torrey Pines Road, BCC-315, La Jolla, CA 92037, USA.

0968-0896/$ - see front matter © 2004 Elsevier Ltd. All rights reserved.
doi:10.1016/j.bmc.2004.11.041

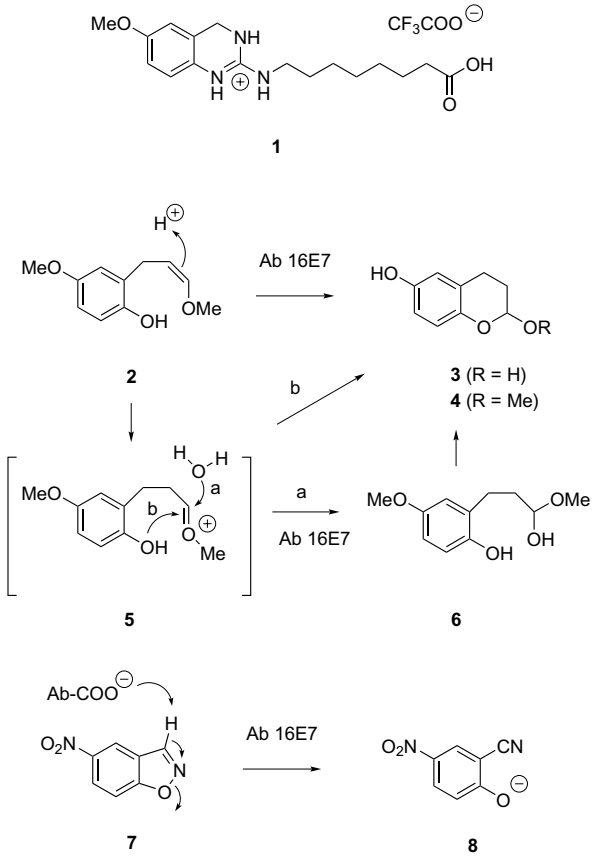

Figure 1. Carbon protonation and deprotonation reaction catalyzed by antibody 16E7 (anti-**1**).

16E7. Furthermore, the modeling study provided a mechanistic hypothesis linking the hysteresis effect to a slow breathing motion of the HCDR3 loop, which was tested by mutagenesis.

2. Materials and methods

2.1. Cloning of antibody 16E7 Fab gene fragment

Total RNA was isolated from the hybridoma cell line 16E7 with RNeasy kit (Qiagen) and its cDNA library was constructed with the Omniscript kit (Qiagen). The Fd and *kappa* chain gene fragments of 16E7 were amplified by PCR with the degenerated primer set as described.[8] Amplified PCR products were digested with XhoI-SpeI for the Fd gene fragment and SacI-XbaI for the *kappa* chain gene fragment, respectively, and ligated into phage display vector pcomb3H[8] to give pcomb3H-16E7. The resulting clone was checked for its affinity to the hapten-BSA conjugate with phage display panning methods.[8] All PCRs were carried out with Vent proofreading polymerase (New England Biolab).

2.2. Construction of chimeric Fab fragment

The VL and VH genes of Ab 16E7 were amplified using pcomb3H-16E7 as the template with the following primers: VL sense, CCAGATGTGAGCTCGTGACCCAGACTCCA (the SacI restriction site is underlined); VL anti-sense, GCAGCATCAGCCCGTTTTATTTCAAGCTTGG (HindIII); VH sense, AGGTCCAGCTGCTCGAGTCTGG (XhoI); VH anti-sense, GAGACGGTGACCAGAGTCCCTTGG (BstEII). The amplified fragments were cloned into appropriate sites in the vector p4xH-M13[9] to give a plasmid in which the VL and VH segments of the antibody 16E7 are fused to human Cκ and gamma1 CH1 regions. The chimeric Fab 16E7 gene fragment was subcloned into pBAD-43C9 vector[10] by PCR with VL sense and CH1 anti-sense primer, CACCGCCGGTCGACTCAGTGGTGGTGGTGGTGGTGTGTGTGAGTTTTGTCAC (SalI), 6XHistidine tag was added at the C-terminus of chimeric Fd. The resulting expression plasmid pBAD-16E7his allows one to express a 6X Histidine containing chimeric Fab 16E7.

2.3. Production, purification, and characterization of chimeric Fab fragments

The *Escherichia coli* strain TOP10 (Invitrogen) was transformed with pBAD-16E7his and its mutagenized derivatives for expression of the wild type and mutant antibodies. 1/40 volume of preculture was inoculated into LB medium containing 100 μg/mL ampicillin at 20 °C and overexpression was performed after induction with 0.1% L(+)-arabinose at OD_{600} of 1.5. 1/10 culture volume of Terrific Broth was added to implement nutrition for overexpression. After 14 h induction, the crude periplasmic lysate was prepared by sonication. The chimeric Fab 16E7 fragment was purified by Ni^{2+} NTA affinity chromatography (Qiagen). Concentrations of purified antibodies were determined by measuring A_{280} and A_{260}.[11] The purity of the sample was confirmed by SDS-PAGE. The same procedure was applied for the production and purification of mutants (see below). WT and mutant chimeric 16E7-Fab fragments were obtained in similar purified yields of 0.6–1.0 mg/L culture.

2.4. Site-directed mutagenesis

Site-directed mutagenesis was accomplished by a QuikChange™ site-directed mutagenesis protocol with minor modification and including silent restriction site. All PCRs were performed with the High Fidelity System (Roche). Mutant codons were generally chosen to exploit the most frequently used codon for a particular amino acid among highly expressed genes in *E. coli*. Oligonucleotides were custom-synthesized and purified by MicroSynth (Balgach, Switzerland) as follows:

D^{H50}A_for GGAGcTATTTACCCTGGAtccGGGAATACTTACTAC (BamHI)
D^{H50}A_rev CCCggaTCCAGGGTAAATAgCTCCAATCCACTCAAGTCC
E^{L39}Q_for CCTATTTAcaATGGTAtCTGCAGAAACCAGGCC (KpnI deletion)
E^{L39}Q_rev GCAGaTACCATtgTAAATAGGTGTTTCCATTAC
E^{L39}A_for CCTATTTAGcATGGTAtCTGCAGAAACCAGGCC (KpnI deletion)

E^{L39}A_rev GCAGaTACCATgCTAAATAGGTGTT-TCCATTAC
S^{H99}A_for GGTACTACGGTgcTGGCGCTGTCTCC-TGGGGC
S^{H99}A_rev CAGCGCCAgcACCGTAGTACCCgCgg-GCACAGAAATAGAC (SacII)
S^{H99}del_for
GGTACTACGGTGGCGCTGTCTCCTGGGGCG
S^{H99}del_rev GAGACAGCGCCACCGTAGTACCCg-CggGCACAGAAATAG (SacII)

For all primers, mutagenized positions are denoted in lowcase. The restriction sites are underlined.

2.5. Kinetic measurements

A solution of antibody in BisTris buffer, pH 6.24 at 37 °C was mixed with a substrate solution (acetonitrile/buffer = 1:1) providing a final solution containing 29 mM BisTris, 104 mM NaCl, 10% acetonitrile. The final antibody concentration was 250–540 μg/mL for the hydrolysis of the enol ether and 24–90 μg/mL for the Kemp elimination. Product formation was followed by RP18-HPLC on a Bischoff LiChrospher 100 (4.6 × 125 mm) column using isocratic elution at 1 mL/min with a premixed acetonitrile/water solution with the desired proportion. The 16E7-catalyzed elimination was followed by measuring A_{380} using a Molecular Devices microtiter plate reader. Measurements were taken at intervals of 60, 90, or 120 s. With all substrates, the antibody-catalyzed reactions were carried out in parallel with an equivalent reaction containing excess hapten **1** (20 μM) for inhibition. All reactions of WT and mutant Fab-16E7 in the presence of hapten **1** gave background level reaction rates, indicating that the observed activities originated from the antigen combining site of the antibodies.

2.6. Data treatment

For the hydrolysis of the enol ether, the values for the initial velocity v_i and for the final velocity v_{ss} were graphically estimated from the slopes of the progress curve. From following equation:

$$T = \frac{(v_{ss} - v_i)}{v_{ss}} \cdot \tau, \qquad (1)$$

the value T of the intercept on the time axis was used to determine the apparent rate constant τ for the transition between the two velocities v_i and v_{ss}.[4,12] For the Kemp elimination the data were analyzed with Kaleidagraph (Abelbeck Software). The three parameters v_i, v_{ss}, and τ were obtained from the following equation:[4,12]

$$[P] = v_{ss} \cdot t - (v_{ss} - v_i) \cdot (1 - e^{-t/\tau}) \cdot \tau. \qquad (2)$$

2.7. Michaelis-Menten kinetics

The hydrolysis of the enol ethers was initiated by adding the substrate to the antibody in a capped microtiter plate. The microtiter plate was kept in a closed plastic box with a wet paper towel inside for humidity saturation at 37 °C. Substrate and product concentrations were measured by RP-C_{18}-HPLC after 12, 20, and 28 h incubation time, allowing to determine the initial velocities v_i and the final velocities v_{ss} for the different substrate concentrations used in the measurements. After correction of these rates for the uncatalyzed reaction rates in BisTris buffer, the net rates v_i and v_{ss} were obtained. These rates were used to derive the Michaelis-Menten constants K_M and the maximum velocity V_{max} from the Lineweaver–Burk plot of $1/V$ versus 1/[S]. The catalytic constant k_{cat} was obtained by dividing V_{max} by the antibody concentration. For the Kemp elimination the obtained velocities v_i and v_{ss} from Eq. (2) were used to determine the value K_M/V_{max} from the Lineweaver–Burk plot of $1/V$ versus 1/[S].

3. Results

3.1. Hysteresis character of chimeric Fab 16E7

Antibody 16E7 was expressed as chimeric Fab in *E. coli* after joining the variable heavy and light chains regions with the human *kappa* chain constant region and heavy chain IgG1 CH1 region, respectively. This chimeric antibody catalyzes both the protonation of enol ether **2** and the deprotonation of benzisoxazole **7** with activity parameters comparable to those of the hybridoma derived IgG antibody, including the hysteresis phenomenon characterized by the retardation time τ, the initial velocity v_i and the steady-state velocity v_{ss} (Table 1). In the case of enol ether **2** the transition between the initial phase of catalysis (v_i) and the steady-state phase of catalysis (v_{ss}) is accompanied by an increase in substrate binding (threefold lower K_M), while the catalytic rate constant k_{cat} is unaffected (Table 2). Only the specificity constant k_{cat}/K_M was determined for benzisoxazole **7** since no substrate saturation occurred within the concentration range accessible with this substrate, and was found to increase by two-fold between the initial phase and the steady-state phase.

3.2. Homology modeling and docking

The 3-D structure of the antibody 16E7 Fv domain was constructed using the online antibody structure modeling service WAM (Web Antibody Modeling, http://antibody.bath.ac.uk/).[13] The whole molecule energy minimization procedure resulted in 200 antibody structures for antibody 16E7, which were ordered with ascending minimization energy. The obtained antibody model was then used in a docking procedure for the different ligands using the docking program AUTODOCK 3.05.[14] All docking attempts with the tight binding hapten **1** or the substrates **2** and **7** failed starting with the lowest energy model 16E7-E1. However, the docking procedure was successful when starting from the second lowest energy model 16E7-E2.

In the resulting model of the antibody–hapten complex, ligand **1** appears to be buried in a very deep pocket located at the center of Fv domain. The hapten is in direct contact with two carboxylate residues, Glu^{L39}

Table 1. The kinetic parameters of antibody 16E7-catalyzed hydrolysis and deprotonation reaction

Antibody	Enol ether **2**[a,b]			Benzisoxazole **7**[a,c]			Benzisoxazole **7**[a,d]		
	v_i (μM h^{-1})	v_{ss} (μM h^{-1})	τ (h)	v_i (μM h^{-1})	v_{ss} (μM h^{-1})	τ (h)	v_i (μM h^{-1})	v_{ss} (μM h^{-1})	τ (h)
MAb 16E7	3.42	5.73	12.15	n.a.	n.a.	n.a.	n.a.	n.a.	n.a.
Fab 16E7	2.79	9.45	12.62	65.8	154.6	0.25	26.3	29.4	3.45
Glu^{L39}Ala	n.a.	n.a.	n.a.	1.95	11.9	1.4	n.a.	n.a.	n.a.
Glu^{L39}Gln	n.a.	n.a.	n.a.	3.12	8.50	0.81	n.a.	n.a.	n.a.
Asp^{H50}Ala	n.a.	n.a.	n.a.	13.39	34.95	0.47	n.a.	n.a.	n.a.
Ser^{H99}Ala	1.12	9.86	7.9	n.a.	n.a.	n.a.	6.11	8.15	1.52
Ser^{H99} deletion	0.35	5.10	7.8	n.a.	n.a.	n.a.	4.79	5.29	2.51

[a] All measurements were carried out with a solution containing antibody in the buffer of 29 mM BisTris, 104 mM NaCl, 10% acetonitrile, pH 6.24 at 37 °C.
[b] The enol ether hydrolysis was performed with an antibody concentration of 0.54 mg/mL and with a substrate concentration of 300 μM.
[c] For the investigation of the catalytic residues all measurements were carried out with an antibody concentration of 0.27 mg/mL and a substrate concentration of 156 μM.
[d] For the investigation of the hysteresis were all measurements carried out with an antibody concentration of 0.09 mg/mL and a substrate concentration of 633 μM.

Table 2. Kinetic parameters for antibody 16E7 catalyzed reactions

Substrates	Enol ether **2**[a]		Benzisoxazole **7**[b]	
	Initial phase[c]	Steady-state phase[d]	Initial phase[e]	Steady-state phase[f]
k_{cat} (s^{-1})	1.00×10^{-3}	1.11×10^{-3}	n.d.	n.d.
k_{uncat} (s^{-1})	7.99×10^{-7}	7.99×10^{-7}	3.62×10^{-6}	3.62×10^{-6}
k_{cat}/k_{uncat}	1262	1392	n.d.	n.d.
K_M (μM)	513	171	n.d.	n.d.
k_{cat}/K_M (μM^{-1} s^{-1})	1.97×10^{-6}	6.47×10^{-6}	4.97×10^{-5}[g]	1.13×10^{-4}[g]
K_S (μM)[h]	0.406	0.124	7.28×10^{-2}	3.20×10^{-2}

[a] All assays were performed at an active site concentration of 3.33 μM.
[b] All assays were performed at an active site concentration of 0.48 μM.
[c] The kinetic parameters were determined after 3 h incubation time.
[d] The kinetic parameters were determined after 15 h incubation time.
[e] The kinetic parameters were determined after 6 min incubation time.
[f] The kinetic parameters were determined after 2 h incubation time.
[g] The low solubility of **7** prevented measurements at substrate concentrations above 2500 μM, without evidence for substrate saturation, hence only k_{cat}/K_M is reported.
[h] K_S is defined as the dissociation constant of the complex between catalyst and the reaction's transition state and can be calculated by following equation: $K_S = k_{uncat}/(k_{cat}/K_M)$.

and Asp^{H50}, which are placed at 9 Å distance from one another (Fig. 2A). The hapten–antibody contact consists mainly in a charge-neutralizing hydrogen bond network involving the negatively charged Glu^{L39}, Tyr^{L41}, and the nitrogen atoms of the cationic guanidinium group of hapten **1**. A similar pair of carboxylates has been observed in the structure of catalytic antibody 4B2, which was obtained against a guanidine-type hapten related to **1** and which also catalyzes the deprotonation of substrate **7**, as well as the deprotonation of a β-γ-unsaturated ketone.[7]

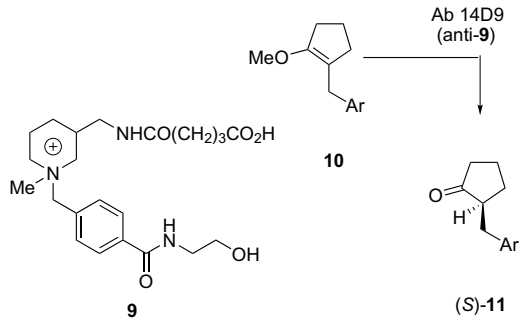

Figure 2. Enol ether protonation reaction with antibody 14D9 raised against hapten **9**.

Enol ether substrate **2** also docked successfully into the Fv domain binding pocket of the 16E7-E2 model (Fig. 2B). The substrate's reactive enol ether function is positioned in proximity of the carboxylate group of Glu^{L39} previously found to interact with the guanidinium group of hapten **1**, with an orientation suitable for proton transfer. Tyr^{L41} forms two hydrogen bonds with Glu^{L39} and the oxygen atom of the substrate's enol ether functional group. The distance of 4.5 Å separating Glu^{L39} from the enol ether β-carbon is analogous to the situation observed in the related catalytic antibody 14D9, an antibody raised against the quaternary ammonium hapten **9** and which catalyzes the enantioselective protonation of enol ethers such as the tranformation of **10** to (*S*)-**11** (Fig. 3). This suggests that a water molecule might be involved in bridging proton transfer between the substrate and the carboxylic acid function of Glu^{L39}. This water molecule might also trap the intermediate

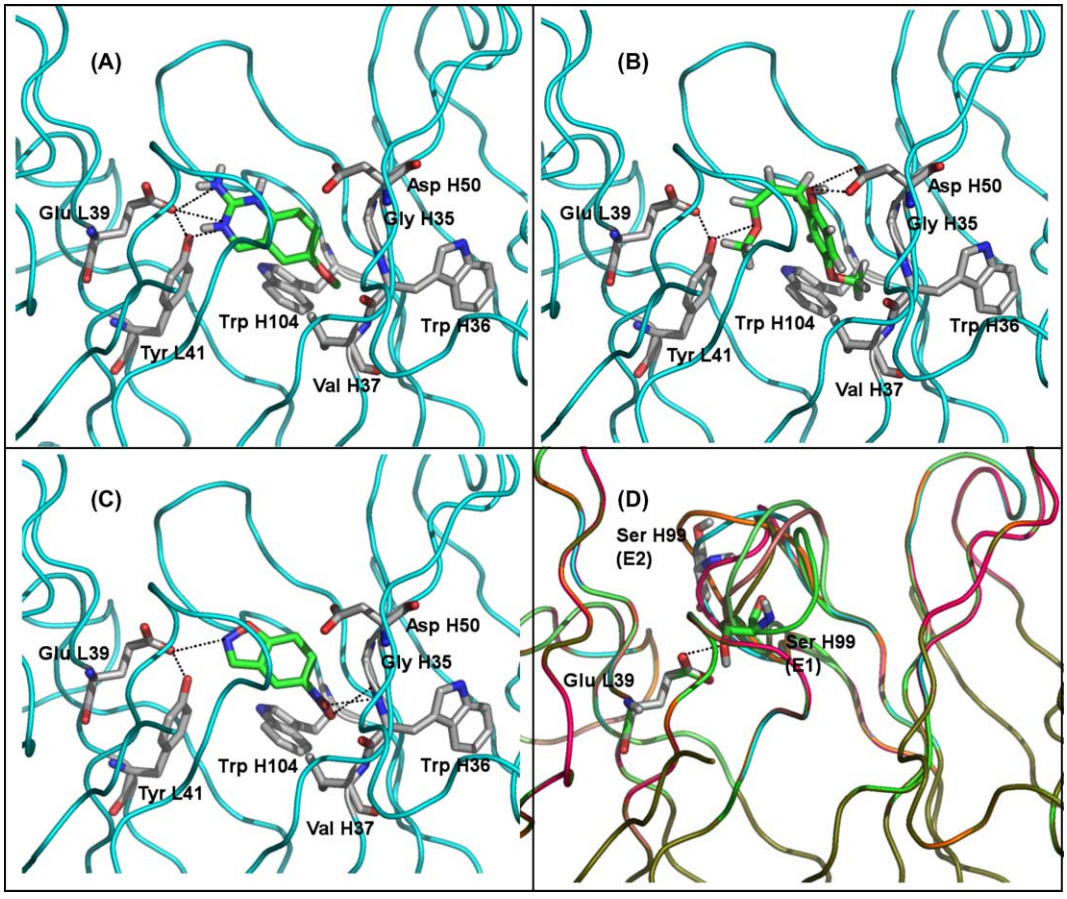

Figure 3. Views of the 16E7 Fv model combining site. The residues in the binding pocket are drawn in gray stick and the ligands are shown in green. (A) Complex with docked hapten **1**. (B) Complex with enol ether substrate **2**. (C) Complex with docked benzisoxazole substrate **7**. (D) HCDR3 flexibility in models 16E7 E1-E7. E1: green; E2: cyan; E3: olive; E4: orange; E5: lime; E6: magenta; E7: salmon. The Glu^{L39} and Ser^{H99} of model E1, E2 are shown in green and gray sticks, respectively.

oxocarbonium cation **5** to form the acyclic hemiacetal **6** as the primary reaction product (Fig. 1). Asp^{H50} forms a hydrogen bond with the phenolic OH-group of substrate **2**, holding this group away from the enol ether function. This orientation might explain the fact that enol ether **2** does not undergo an intramolecular cyclization to the corresponding acetal **4** under antibody catalysis, but rather undergoes hydrolysis to **3** as observed in the background reaction in water.

Benzisoxazole **7** also docked into 16E7-E2 model to produce a stable complex (Fig. 2C). In this case, the critical acidic residue Glu^{L39} forms two hydrogen bonds, one with Tyr^{L41}, and another with the nitrogen atom in the substrate's benzisoxazole ring. The substrate's deprotonation site is located at a distance of 3 Å from the carboxylate of Glu^{L39} in an arrangement suitable for direct proton transfer.

3.3. Mutagenesis of catalytic residues

Mutagenesis experiments suggested by the modeling and docking study were carried out to probe the reaction mechanism of antibody 16E7 (Table 1). The role of Glu^{L39}, which appeared as the best candidate for a catalytic residue, was investigated first. Mutation of Glu^{L39} to either glutamine or alanine abolished catalytic activity in both, the protonation reaction with enol ether **2** and the deprotonation reaction with benzisoxazole **7**, establishing that this residue is critical for catalysis in antibody 16E7. Residue Asp^{H50} was mutated to alanine to remove its hydrogen-bonding interaction with the phenolic hydroxyl group of enol ether **2** as observed in the docked model (Fig. 2A), with the hope that the $Asp^{H50}Ala$ mutant might promote an intramolecular cyclization of enol ether **2** to form the cyclic acetal **4**. Unfortunately, the $Asp^{H50}Ala$ mutant was completely inactive for the protonation reaction. Nevertheless, this mutant retained 25% of the WT activity for the deprotonation reaction with benzisoxazole **7**. The selective loss of catalysis for the enol ether reaction suggests that this reaction is more sensitive to perturbations than the Kemp's elimination reaction of benzisoxazole **7**, in agreement with the fact that the later reaction is very sensitive to non-specific catalysis effects.[16] The loss of activity in the case of enol ether **2** might be due to perturbed substrate binding.

3.4. Analysis of loop movements

The fact that docking hapten **1** or the substrates onto the lowest energy 16E7-E1 model did not produce a

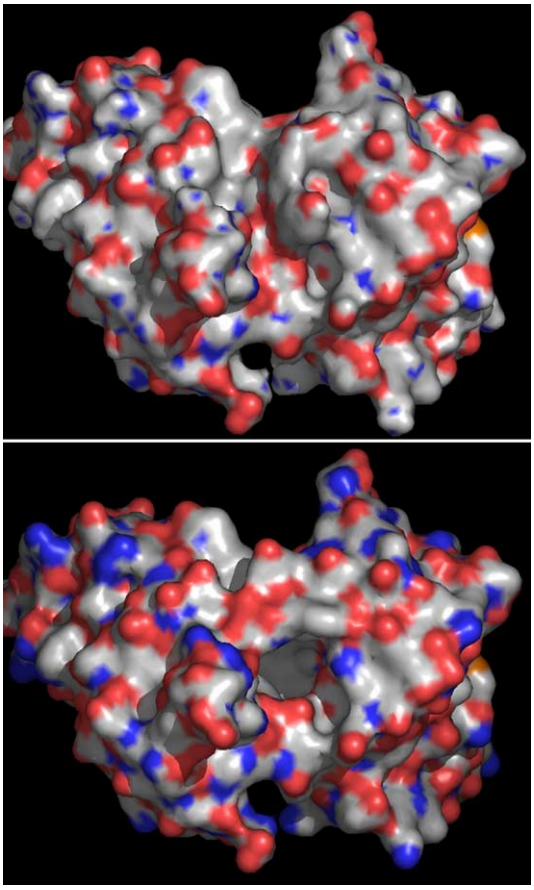

Figure 4. Comparsion of 16E7 models molecular surface. Top: the 16E7-E1 model, bottom: the 16E7-E2 model.

complex suggested that the ligands could not enter the binding pocket in this model. Indeed AUTODOCK 3.05 employs a molecule 'walking' procedure on the surface of the molecule to search the potential binding pocket. The structural difference between the 16E7-E1 model and the 16E7-E2 model used to produce docked complexes was identified as a large conformational change in the HCDR3 loop. In the 16E7-E1 model, this loop closes the binding pocket unusually deeply, preventing ligand access. In the 16E7-E2 model, by contrast, the loop is placed such as to leave the pocket open (Fig. 4).

The five next lower energy models for 16E7 were examined. These were found to represent intermediate states of a loop movement between the 16E7-E1 and the 16E7-E2 conformation (Fig. 2D). The HCDR3 loop movement involved seven contiguous residues (Tyr^{H96}-Gly^{H97}-Gly^{H98}-Ser^{H99}-Ala^{H100}-Val^{H101}-Ser^{H102}) and featured a rotation spanning 67° as measured for the Cα atom of Gly^{H98} in relation to the Cα atom of Arg^{H95} as fixed point. The calculated energy difference between E1 and the least stable of these seven conformers amounted to 4.8 kcal/mol, suggesting that the loop rearrangement required a significant activation energy (Table 3). Further examination of the 50 lowest energy conformers showed that the HCDR3 loop was more flexible compared to its LCDR3 counterpart (Fig. 5).

Table 3. The conformation characters of HCDR3 with increasing energy

Energy minimization conformation	ΔG (kcal/mol)	Loop flexibility (deg)
E1	0	0
E2	1.30	67.64
E3	2.07	33.47
E4	4.22	54.21
E5	4.48	47.68
E6	4.65	42.03
E7	4.82	23.15

E1–E7 are the generated conformations during whole molecular minimization and ordered by increasing energies. ΔG is the energy difference between every conformation and the minimized conformation. Loop angles were measured with the program *Swisspdbviewer*. The Cα atom of $Glycine^{H98}$ in the HCDR3 conformation of E1 was chosen as reference point and defined as an angle of 0°. Angles are defined for the motion of the Cα atom of Gly^{H98} in relation to the Cα atom of Arg^{H95} as fixed point.

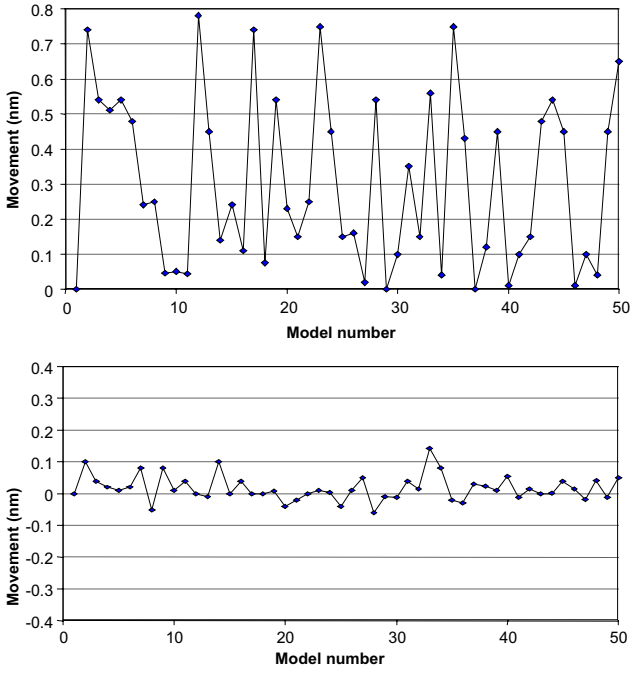

Figure 5. Scalar representation of CDR3 loops flexibility of 16E7 Fv models E1–E50. Two atoms on the tip of the CDR3 loops of heavy and light chain were used to calculate the movement of their loops. Top: Cα atom of the Gly^{H98}, bottom: Cα atom of Val^{L99}. Their positions in the E1 model are set to zero and compared to the corresponding atoms in the conformations of the other models.

3.5. Mutagenesis of Serine H99

The movement of the HCDR3 observed between the 16E7-E1 model and the 16E7-E2 model might explain the hysteresis behavior of antibody 16E7. Indeed, the substrates might meet a similar entry problem in the real antibody to that observed in the docking procedure with the 16E7-E1 model. Thus, the 16E7-E1 model might represent a conformation existing in the catalytic antibody during the initial kinetic phase (v_i), while the 16E7-E2 model might represent the antibody conformation during the activated state of the kinetic phase (v_{ss}).

Since Ser^{H99} played a crucial role in locking the closed conformation of the 16E7-E1 model by hydrogen-bonding interactions with Glu^{L39}, we reasoned that mutating this residue to an alanine might destabilize the inactive state of antibody 16E7 and therefore reduce the activation time τ for reaching full activity. Substituting alanine for serine at position H99 produced a catalytically active mutant for both the protonation of enol ether **2** and the deprotonation of benzisoxazole **7**, showing approximately 25% of WT activity in both cases. More importantly, the hysteresis time τ in the Ser^{H99}Ala mutant was reduced to 44% of WT for the reaction of benzisoxazole **7**, and to 62% of WT for the protonation of enol ether **2** (Table 1, Fig. 6). Similar reductions in hysteresis were observed when Ser^{H99} was deleted. These effects are consistent with the mechanistic hypothesis assigning the hysteresis behavior to a movement of the HCDR3 loop between a more stable, catalytically less active conformer (model 16E7-E1) and a slightly less stable, catalytically more active conformer (model 16E7-E2), taking place in a slow transition requiring a significant activation energy.

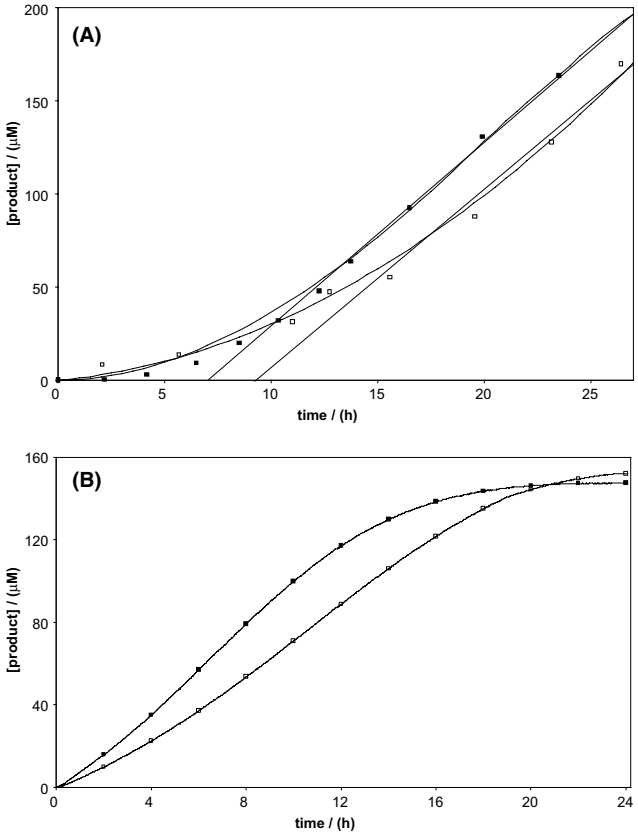

Figure 6. Hysteresis effect in catalytic antibody 16E7. (A) Hydrolysis of the enol ether **2**. Hysteresis observed for WT Fab-16E7 (□) and for the mutated Fab-16E7(Ser^{H99}Ala) (■). The values for the initial velocity v_i and final velocity v_{ss} are fitted according to the equation described in the literature.[4,12] Assays were performed at an initial substrate concentration of 300 μM and an antibody concentration of 0.54 mg/mL (29 mM BisTris, 104 mM NaCl, 10% acetonitrile, pH 6.24, 37 °C). (B) Observed hysteresis of the chimeric WT Fab 16E7-catalyzed (□) and of the Fab-16E7 (Ser^{H99}Ala)-catalyzed (■) elimination of the Kemp substrate **7**. Assays were performed at an initial substrate concentration of 475 μM and an antibody concentration of 0.09 mg/mL (29 mM BisTris, 104 mM NaCl, 10% acetonitrile, pH 6.24, 37 °C).

4. Discussion

4.1. Homology modeling and docking

Homology modeling has been used broadly for antibodies[17] and the validity of the models produced has been confirmed in several cases by crystallographic studies.[18] Computational simulations have also been used extensively to analyze protein dynamics,[19] and the results confirmed by fluorescence,[20] CD spectroscopy and NMR studies.[21] While the overall structure of antibodies is largely conserved, modeling concentrates on predicting the conformation of the CDR in the active site. In this study we used the online antibody structure modeling service WAM (Web Antibody Modeling, http://antibody.bath.ac.uk/),[13] which uses a combination of sequence comparison and conformation searches for predicting the three-dimensional structure from sequence data. In order to probe the reliability of this service we submitted the sequence of catalytic antibody 14D9 from our group prior to its publication.[15] In this case we obtained a modeled structure, which was very close to the actual structure as observed in the crystal structure, showing that the model is capable of accurate predictions for antibodies raised against small molecule haptens. Docking of ligands into the 16E7 model was accomplished using the docking program AUTODOCK 3.05[14] This program has been described to be generally suitable for elucidating interactions between antibodies and ligands.[22] In the present study modeling and docking were used as a guide for selecting mutagenesis experiments to probe the reaction mechanism and hysteresis effect.

4.2. Catalytic mechanism of antibody 16E7

The mechanism of proton transfer to and from carbon in enzyme catalysis is of particular interest since this step is generally kinetically slow and may be rate limiting in a catalytic cycle. The data above for antibody 16E7 clearly point to Glu^{L39} as the key catalytic residue responsible for both the protonation catalysis with enol ether **2** and the deprotonation catalysis with benzisoxazole **7**. The direct carbon deprotonation reaction of substrate **7** by Glu^{L39} proposed here for antibody 16E7 is similar to the general base mechanism proposed for catalytic antibody 2B4 on the basis of its crystal structure.[7] On the other hand, we observed a distance of 4.5 Å between the catalytic carboxyl group of Glu^{L39} and the β-carbon of enol ether **2** in the docked model of 16E7. This situation is analogous to that observed in the crystal structure of catalytic antibody 14D9, which also catalyzes an enol ether protonation reaction, suggesting a similar mechanism with an intervening water molecule.[15] The data with antibody 16E7 thus bridges both situations and suggests a common mechanism for proton transfer to and from carbon in catalytic antibodies. The situation is also similar in several enzymes where glutamate

residues have been found to catalyze protonation or deprotonation reactions.[7,23]

The hydrogen-bonding interaction between the phenolic hydroxyl group of substrate **2** and Asp^{H50} observed in the docked model of antibody 16E7 with the enol ether, which places this phenolic hydroxyl group away from the enol ether, provides a structural model to explain the exclusive trapping of the intermediate carbocation by water, which takes place in the antibody catalysis despite of the desolvation occurring upon substrate binding. Desolvation should indeed rather favor an intramolecular cyclization pathway to acetal **4**, as observed upon treatment of enol ether **2** with strong acid under non-aqueous conditions.[4] The binding conformation of substrate **2** in the docked model is also in agreement with the observation that antibody 16E7 is not inhibited by product **3** and its cyclic acetal analog **4**, an observation which alone suggests that the binding pocket is not suited for forming the cyclized product.

4.3. Hysteresis effect

Hysteresis effects in catalysis have been observed and characterized in several enzymes and linked to protein motions such as loop movements and quaternary conformational rearrangements. These phenomena are referred to as 'protein breathing' when their time scale is on the order of several hours.[24,25] Antibodies have also been shown to display protein dynamics effects ranging from adjustment of a single amino acid side chain[26] and loop rearrangements[27] to entire domain movements.[28] By contrast, catalytic antibodies have been generally regarded as possessing a relatively rigid binding pocket, and numerous crystal structures of catalytic antibodies show no significant differences between apo- and hapten-bound structures.[29] A study by Tawfik and co-workers suggested that a protein conformational change might be responsible for a relatively short hysteresis effect, observed as a delay of a few tens of seconds, in the activation of a catalytic antibody upon substrate binding.[30] The protein dynamical aspects of antibody binding have been recently demonstrated by the same authors by the crystallographic observation of two isolable distinct conformations of a single antibody binding to two different haptens.[31]

The homology modeling suggests that the unusual hysteresis in antibody 16E7 catalysis, which is observed with both substrates, originates in a slow conformational movement of the HCDR3 loop switching from a closed conformation blocking substrate access to the catalytic site (16E7-E1 model) to a catalytically active open conformation (16E7-E2 model). This mechanism is supported by the 38–56% reduction in hysteresis time observed in the $Ser^{H99}Ala$ and the Ser^{H99} deletion mutants (Table 1). This effect can be interpreted in terms of residue Ser^{H99} locking the closed conformation by hydrogen bonding to Glu^{L39} as suggested by the model. Interestingly models E3 to E7 displaying intermediate states of the loop movement have a significantly higher calculated energy relative to E1 and E2, which is consistent with the slow hysteresis if attributed to the modeled conformational rearrangement between E1 and E2. However, the energy barrier of 4.8 kcal/mol given by the model is not sufficient to quantitatively explain the very long activation times observed. The modeled conformational rearrangement is also consistent with the threefold tighter binding of enol ether **2** in the steady state (open conformer E2) versus initial phase (closed conformed E1). Although the K_M values are not accessible, the twofold higher activity with benzisoxazole **7** in the steady state versus initial phase might also be caused by tighter substrate binding.

Induced-fit upon ligand binding and pre-equilibrium have been considered as driving forces for conformational changes in several hysteresis enzymes and antibodies.[27,30,32] In the present case of antibody 16E7, the closed, catalytically inactive E1 conformation could be favored in the absence of substrate. The open E2 conformation would represent the tighter binding conformation, and would exist mainly with bound ligands. The substrate–antibody interaction in this model may be described either as induced-fit or as pre-equilibrium depending on whether the conformational rearrangement occurs with or without bound substrate. In any event this two-state model is consistent with the fact that the constant τ decreases upon increasing substrate concentration, and with the fact that the inactive state is regenerated upon repurification of the antibody by protein G affinity chromatography.

5. Conclusion

The mechanistic model proposed on the basis of site-directed mutagenesis and molecular modeling provides a consistent picture of the mechanism of proton transfer to and from carbon in catalytic antibody 16E7. Mutagenesis of the key residues Glu^{L39}, Asp^{H50}, and Ser^{H99} shows that these residues control the catalysis and hysteresis phenomenon of the antibody. Proton transfer depends on Glu^{L39} and proceeds analogously to proton transfer steps observed in related systems, which supports a common mechanism for proton transfer in catalytic antibodies. The unusual hysteresis of antibody 16E7 might be explained by a slow conformational movement of the HCDR3 loop.

Acknowledgements

This work was supported by the Swiss National Science Foundation, the University of Basel, and the University of Berne.

References and notes

1. Schultz, P. G.; Yin, J.; Lerner, R. A. *Angew. Chem., Int. Ed.* **2002**, *41*, 4427–4437.
2. Stevenson, J. D.; Thomas, N. R. *Nat. Prod. Rep.* **2000**, *17*, 535–537.
3. Kemp, D. S. *Nature* **1995**, *373*, 196–197.

4. Manetsch, R.; Zheng, L.; Reymond, M. T.; Woggon, W.-D.; Reymond, J.-L. *Chem. Eur. J.* **2004**, *10*, 2487–2506.
5. Reymond, J.-L.; Jahanghiri, G. K.; Stoudt, C.; Lerner, R. A. *J. Am. Chem. Soc.* **1993**, *115*, 3909–3917.
6. Thorn, S. N.; Daniels, R. G.; Auditor, M.-T. M.; Hilvert, D. *Nature* **1995**, *373*, 228–230.
7. Golinelli-Pimpaneau, B.; Goncalves, O.; Dintinger, T.; Blanchard, D.; Knossow, M.; Tellier, C. *Proc. Natl. Acad. Sci. U.S.A.* **2000**, *97*, 9892–9895.
8. Barbas, C. F.; Kang, A. S.; Lerner, R. A.; Benkovic, S. J. *Proc. Natl. Acad. Sci. U.S.A.* **1991**, *88*, 7978–7982.
9. Ulrich, H. D.; Patten, P. A.; Yang, P. L.; Romesberg, F. E.; Schultz, P. G. *Proc. Natl. Acad. Sci. U.S.A.* **1995**, *92*, 11907–11911.
10. Yin, J.; Mundorff, E. C.; Yang, P. L.; Wendt, K. U.; Hanway, D.; Stevens, R. C.; Schultz, P. G. *Biochemistry* **2001**, *40*, 10764–10773.
11. Harlow, E.; Lane, D. *Antibodies: A Laboratory Manual*; Cold Spring Harbor Lab. Press: Plainview, NY, 1988.
12. Neet, K. E.; Ainslie, R. *Methods Enzymol.* **1980**, *64*, 192–226.
13. Whitelegg, N. R. J.; Rees, A. R. *Protein Eng.* **2000**, *13*, 819–824.
14. Morris, G. M.; Goodsell, D. S.; Halliday, R. S.; Huey, R.; Hart, W. E.; Belew, R. K.; Olson, A. J. *J. Comput. Chem.* **1998**, *19*, 1639–1662.
15. Zheng, L.; Baumann, U.; Reymond, J.-L. *Proc. Natl. Acad. Sci. U.S.A.* **2004**, *101*, 3387–3392.
16. Kirby, A. J.; Hollfelder, F.; Tawfik, D. S. *Appl. Biochem. Biotechnol.* **2000**, *83*, 173–180.
17. (a) Roberts, V. A.; Stewart, J. D.; Benkovic, S. J.; Getzoff, E. D. *J. Mol. Biol.* **1994**, *235*, 1098–1116; (b) Miyashita, H.; Hara, T.; Tanimura, R.; Fukuyama, S.; Cagnon, C.; Kohara, A.; Fujii, I. *J. Mol. Biol.* **1997**, *267*, 1247–1257; (c) Stewart, J. D.; Roberts, V. A.; Thomas, N. R.; Getzoff, E. D.; Benkovic, S. J. *Biochemistry* **1994**, *33*, 1994–2003; (d) Fujii, I.; Tanaka, F.; Miyashita, H.; Tanimura, R.; Kinoshita, K. *J. Am. Chem. Soc.* **1995**, *117*, 6199–6209.
18. (a) Thayer, M. M.; Olender, E. H.; Arvai, A. S.; Koike, C. K.; Canestrelli, I. L.; Stewart, J. D.; Benkovic, S. J.; Getzoff, E. D.; Roberts, V. A. *J. Mol. Biol.* **1999**, *291*, 329–345; (b) Kristensen, O.; Vassylyev, D. G.; Tanaka, F.; Morikawa, K.; Fujii, I. *J. Mol. Biol.* **1998**, *281*, 501–511; (c) Smithrud, D. B.; Benkovic, P. A.; Benkovic, S. J.; Roberts, V. A., III; Liu, J.; Neagu, I.; Iwama, S.; Phillips, B. W.; Smith, A. B., III; Hirschmann, R. *Proc. Natl. Acad. Sci. U.S.A.* **2000**, *97*, 1953–1958; (d) Kolesnikov, A. V.; Kozyr, A. V.; Alexandrova, E. S.; Koralewski, F.; Demin, A. V.; Titov, M. I.; Avalle, B.; Tramontano, A.; Paul, S.; Thomas, D.; Gabibov, A. G.; Friboulet, A. *Proc. Natl. Acad. Sci. U.S.A.* **2000**, *97*, 13526–13531.
19. Hansson, T.; Oostenbrink, C.; Van Gunsteren, W. *Curr. Opin. Struct. Biol.* **2002**, *12*, 190–196.
20. Chattopadhyay, K.; Saffarian, S.; Elson, E. L.; Frieden, C. *Proc. Natl. Acad. Sci. U.S.A.* **2002**, *99*, 14171–14176.
21. Kroon, G.; Martinez-Yamout, M.; Krebs, J. F.; Chung, J.; Dyson, H. J.; Wright, P. E. *J. Biomol. NMR* **1999**, *15*, 83.
22. (a) Sotriffer, C. A.; Flader, W.; Winger, R. H.; Rode, B. M.; Liedl, K. R.; Varga, J. M. *Methods: Companion Methods Enzymol.* **2000**, *20*, 280–291; (b) Heine, A.; Stura, E. A.; Yli-Kauhaluoma, J. T.; Gao, C.; Deng, Q.; Beno, B. R.; Houk, K. N.; Janda, K. D.; Wilson, I. A. *Science* **1998**, *279*, 1934–1940.
23. Mitra, B.; Kallarakal, A. T.; Kozarich, J. W.; Gerlt, J. A.; Clifton, J. G.; Petsko, G. A.; Kenyon, G. L. *Biochemistry* **1995**, *34*, 2777–2787.
24. Cannon, W. R.; Benkovic, S. J. *J. Biol. Chem.* **1998**, *273*, 26257–26260.
25. Frieden, C. *Annu. Rev. Biochem.* **1979**, *48*, 471–489.
26. Stanfield, R. L.; Fieser, T. M.; Lerner, R. A.; Wilson, I. A. *Science* **1990**, *248*, 712–719.
27. Rini, J. M.; Schulze-Gahmen, U.; Wilson, I. A. *Science* **1992**, *255*, 959–965.
28. Guddat, L. W.; Shan, L.; Broomell, C.; Ramsland, P. A.; Fan, Z.; Anchin, J. M.; Linthicum, D. S.; Edmundson, A. B. *J. Mol. Biol.* **2000**, *302*, 853–872.
29. (a) Hugot, M.; Bensel, N.; Vogel, M.; Reymond, M. T.; Stadler, B.; Reymond, J.-L.; Baumann, U. *Proc. Natl. Acad. Sci. U.S.A.* **2002**, *99*, 9674–9678; (b) Wedemayer, G. J.; Patten, P. A.; Wang, L. H.; Schultz, P. G.; Stevens, R. C. *Science* **1997**, *276*, 1665–1669; (c) Gigant, B.; Charbonnier, J. B.; Eshhar, Z.; Green, B. S.; Knossow, M. *Proc. Natl. Acad. Sci. U.S.A.* **1999**, *94*, 7857–7861.
30. Lindner, A. B.; Eshhar, Z.; Tawfik, D. S. *J. Mol. Biol.* **1999**, *285*, 421–430.
31. James, L. C.; Roversi, P.; Tawfik, D. S. *Science* **2003**, *299*, 1362–1367.
32. Jaaskelainen, S.; Verma, C. S.; Hubbard, R. E.; Linko, P.; Caves, L. S. *Protein Sci.* **1998**, *7*, 1359–1367.